

PHYSIQUE DE LA MATIÈRE EN GRAINS
PHYSICS OF GRANULAR MEDIA

**From a grain to avalanches:
on the physics of granular surface flows**

Stéphane Douady*, Bruno Andreotti, Adrian Daerr, Pierre Cladé

Laboratoire de physique statistique de l'École normale supérieure
(associé au CNRS et aux Universités Paris 6 et 7), 24, rue Lhomond, 75231 Paris cedex 05, France

Received 6 October 2001; accepted 11 December 2001

Note presented by Guy Laval.

Abstract

Granular surface flows have still to be fully modelled. Analysing the motion of a single grain can already help us to understand the physical origin of several characteristic angles (starting, stopping, jumping angles). Then looking at layers of grains allows the inference of the velocity profile inside the flowing layer, and the physical origin of the flow depth selection. Then these results can be plugged into a general model of mass and momentum conservation integrated vertically (St-Venant). This model can be tested on stationary flows, but also on transients, such as avalanches. *To cite this article: S. Douady et al., C. R. Physique 3 (2002) 177–186.* © 2002 Académie des sciences/Éditions scientifiques et médicales Elsevier SAS

granular flow / friction angle hysteresis / non-local, inelastic shocks / St-Venant equations / avalanche fronts

**D'un grain aux avalanches : sur la physique des écoulements
granulaires de surface**

Résumé

Les écoulements granulaires de surface restent à modéliser. L'analyse du mouvement d'un seul grain permet déjà de comprendre l'origine physique de plusieurs angles caractéristiques (de démarrage, d'arrêt, de saut). Le mouvement de couches de grains explique ensuite le profil de vitesse dans la partie en écoulement et le mécanisme physique de sélection de sa profondeur. Ces résultats peuvent être introduits dans un modèle général de conservation de la masse et de l'impulsion intégrée dans la hauteur (St-Venant). Le modèle peut alors être testé sur des écoulements stationnaires ou transitoires, comme les avalanches. *Pour citer cet article : S. Douady et al., C. R. Physique 3 (2002) 177–186.* © 2002 Académie des sciences/Éditions scientifiques et médicales Elsevier SAS

écoulement granulaire / hysteresis des angles de friction / chocs inélastiques, non locaux / équations de St-Venant / fronts d'avalanches

* Correspondence and reprints.

E-mail address: douady@lps.ens.fr (S. Douady).

1. Introduction

With its ubiquity and practical importance, it is surprising that granular surface flows have not yet been described as clearly and completely as has been done a long time ago for liquid flows. One reason may be that the physical mechanisms at work in the flowing granular layer are different enough from the liquid case, and are hardly described yet. To investigate these mechanisms a first step is to look at the motion of a single grain (Section 2). This already gives many clues to the essential physical mechanisms, namely inelastic collisions and trapping, leading to a strong sub-critical bifurcation between motion and rest [1].

A second step is to look at layers of grains flowing one above the others (Section 3). In this case we have the same effects as for a single grain (inelastic collisions and trapping), but we also find an essential effect: the non-locality of the collisions. This non-locality of the shocks explains the otherwise surprising linear velocity profile, and its combination with the trapping gives the depth selection of the surface flow [2].

From these observations, and other experimental ones, we proposed a model [3]. In Section 4 we compare it with other possibilities [4–10]. Then we present the first comparison of this model with experiments, not on stationary flows [8–12], but on unstationary ones (avalanches) [13–15] (Section 5). We offer possible model verifications in the future.

2. The motion of a single grain

A bead (in practice a cylinder) placed on a row of identical beads presents several states (Fig. 1). The first one is the static equilibrium, when the bead is trapped in the hole in between the beads underneath. If the row of beads is tilted by an angle ϕ , this bead remains static up to the angle at which the trap disappears. The bead will then spontaneously start to roll down. This defines the starting angle ϕ_s (usually referred as the static angle).

Another possible state is to have the bead rolling down indefinitely. Experimentally it reaches quickly a constant mean velocity [16,17]. If the angle of the row is decreased, this periodic motion abruptly becomes impossible below a second lower angle, the stopping angle ϕ_d (usually referred as the dynamical angle).

Analysis of the motion [1] shows that the bead rolls on the underneath ones, without sliding or jumping (for a not too large angle). During its rolling it gains kinetic energy: $\dot{\theta}_{\text{down}}^2 = \dot{\theta}_{\text{up}}^2 + 2\alpha^2(g/d) \sin \phi_s \sin \phi$, where α is related to the ratio of potential energy transferred into translation and rotation kinetic energy, respectively. Then it collides with the next bead. Even though the materials used are not completely inelastic (for instance steel), we do not observe any rebound, but rather a perfectly inelastic normal collision. This perfectly inelastic normal shock can be interpreted as the signature of an inelastic collapse: it makes a small rebound, but then an infinite number of small rebounds in a short finite time. After the shock, there remains some tangential velocity, and also part of the rotation energy is transformed into tangential kinetic energy.

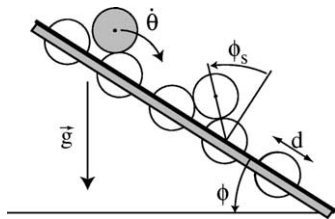


Figure 1. Schematic setup with notations of the single bead experiment.

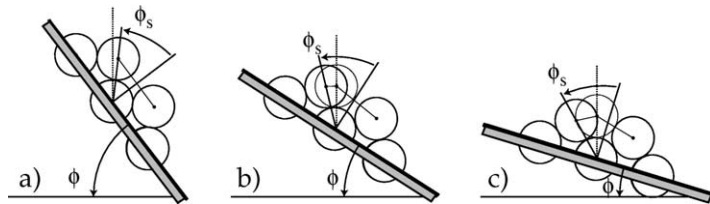


Figure 2. (a) For an angle $\phi > \phi_s$ the bead starts rolling spontaneously; (b) below $\phi < \phi_s$, it can remain static but also, when pushed, reach a constant velocity regime, gaining kinetic energy from potential energy, loosing it at the shocks; (c) further down, $\phi \ll \phi_s$, the gain in potential energy while rolling down reduces while the height above which it has to pass increases. This lead to ϕ_d , the angle below which it has not enough kinetic energy in the limit regime to escape from this trapping, and then stops back.

The bead thus starts rolling on the next bead, with a new angular velocity given by: $\dot{\theta}_{\text{after}} = \rho \dot{\theta}_{\text{before}}$, where ρ (of the order of 1/2) is the restitution coefficient describing the loss of kinetic energy in the shock.

This motion leads quickly to a constant angular velocity:

$$\dot{\theta}_l = \beta \sqrt{\frac{g \sin \phi}{d}} \quad \text{with} \quad \beta = \alpha \rho \sqrt{\frac{2 \sin \phi_s}{1 - \rho^2}}. \quad (1)$$

We can see that this limit angular velocity is far from the mean velocity experimentally observed (cf. Fig. 3). The main difference is that no bead motion is observed below ϕ_d , and clearly not down to an horizontal row ($\phi = 0$). This comes simply from the fact that even if a bead has a non zero angular velocity after one shock, it will not necessarily go down to the next dip: in between the two dips it has to pass above the bead. When the bead row angle is decreased, the limit angular velocity decreases. At the same time, the height above which it has to pass (the trapping height) increases (see Fig. 2). Then comes an angle for which this limit angular velocity is not large enough to escape from the trap, and this explains the origin of ϕ_d . Just above this angle, the bead slows down infinitely when passing above the underneath one, so the mean bead velocity goes abruptly to zero.

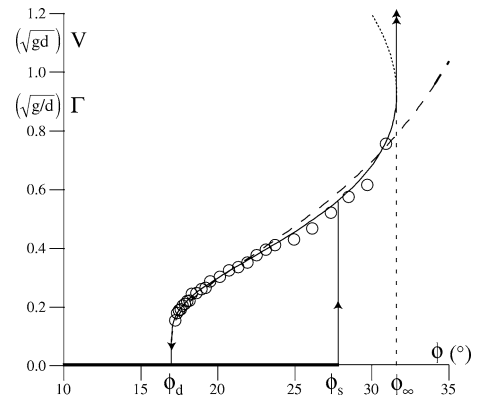
If the bead motion above the underneath beads is numerically integrated, the experimental velocities are well reproduced (Fig. 3). This constant velocity regime ends at an upper angle ϕ_∞ . Slightly below this value, the bead has a too large angular velocity, so that just before a collision it stops rolling, takes off and simply jumps straightforward. The next collision occurs more tangentially, the loss of normal velocity is reduced, hence a larger mean velocity. At ϕ_∞ , the bead starts even to jump above the following bead. It then makes a longer way down before the next collision, transferring more potential energy into kinetic energy, and thus makes a next longer jump, and so on. As a result, the bead accelerates indefinitely.

Far from the previous formula, Eq. (1), a good fit of the mean (macroscopic) velocity is rather given by:

$$V = \gamma \sqrt{gd} / \ln \left(\frac{\tan \phi_\infty - \tan \phi_d}{\tan \phi - \tan \phi_d} \right) \quad (2)$$

with γ of the order of 0.4. However, with this formula, the fitted value for ϕ_∞ is too large and the divergence too slow (long dashed line in Fig. 3) compared to experiment. To be closer to measurements we have to take into account an upper unstable branch (dotted curve).

Figure 3. Mean velocity for a single bead V . Assuming this is the relative layer velocity, it also corresponds to the velocity gradient $\Gamma = V/d$, with d the bead diameter. The bead can stay at rest up to ϕ_s . Then it rolls down at a constant velocity. If the angle is reduced, this constant motion ceases to exist below a second angle ϕ_d . This experiment also reveals a third angle, ϕ_∞ , above which the bead indefinitely accelerates. The exact value of the angles depends on the geometry. In the pure 2D geometry we have $\phi_s > \phi_\infty$, while this is the contrary in 3D. For actual sand piles, the two angles ϕ_d and ϕ_s are closer than in this diagram, and depend on the material. But the typical velocity (or gradient) keeps the same value, around 0.4 in g, d units.



We can also look at the transients leading to this mean velocity, i.e. to the apparent forces acting on the bead. The measurements [1] give a force of the form:

$$F = \sigma g(\sin \phi - \mu \cos \phi) - \kappa \frac{V^2}{d}. \quad (3)$$

The effect of the collisions thus corresponds to a Bagnold type of term, as it should be, the shocks dissipating a part of the velocity V with a frequency V/d [18]. The driving force is in first approximation a force proportional to the gravity force (but smaller than its projection along the beads row). It is striking to see that a friction force also spontaneously appears with a friction coefficient μ . By setting this force to zero, we should recover the mean velocity, as done by Khakhar [10]. This is correct for the central range: this fit does not extend close to ϕ_∞ , and the observed cut-off is sharper ($\mu < \tan \phi_d$).

3. The motion of layers of grains

How can we go from the motion of one bead to the propagation of an avalanche? The next step can be to look at the motion of superposed layers of beads. Even if it is difficult to do it experimentally with rigid layers, we can still turn to numerical simulations. We thus consider layers of periodic beads as sketched in Fig. 4. We assume the same motion than previously: each bead rolls without sliding on the underneath ones.

The crucial assumption concerns the shocks, when a bead in one layer collides with the one underneath in a local shear flow $\partial_z v$. The assumption used for liquids as well as by Bagnold is that the exchange of momentum is local, affecting only the two layers involved in the collision. In the case of liquids, the frequency of shocks is related to thermal agitation. This gives a shear stress:

$$\tau = \nu \partial_z v \quad (4)$$

where ν is the fluid viscosity and v the tangential velocity. With grains, the frequency of shocks comes from the motion of the grains themselves, at a frequency $\partial_z v/d$. This gives the Bagnold's stress:

$$\tau = \kappa d^2 (\partial_z v)^2 \quad (5)$$

where κ is a geometric constant. The characteristics of both resulting velocity profile are their positive curvature, the fact that the velocity derivative is null at the free surface (where no stress is exerted), and to flow down to the bottom, as sketched on Fig. 5, (b) and (c).

Here, the main problem is precisely to model a surface flow, i.e. only a thin flow of grains on a remaining static layer (Fig. 5(a)). In our model, the beads are always rolling one above another, so they are always in

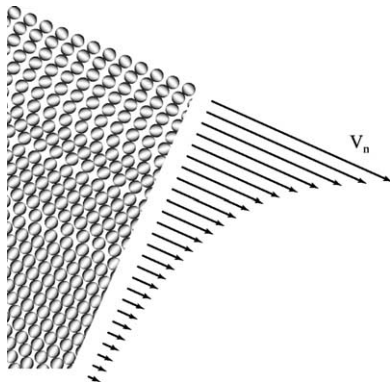


Figure 4. Sketch of the flowing layers at one moment of their motion (left), with the resulting mean velocity profile (right).

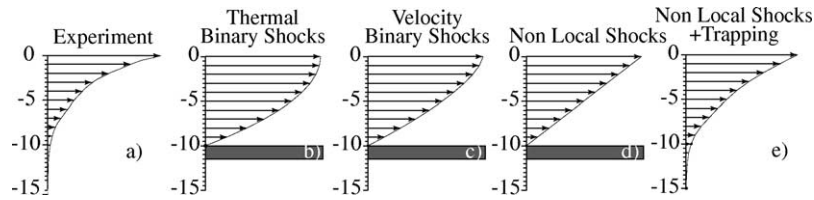


Figure 5. Types of velocity profiles: (a) as experimentally observed using PIV, (b) with thermally induced binary shocks (viscous fluid), (c) with binary shocks induced by the motion itself (Bagnold’s profile), (d) with non-local shocks in connected grains (this layer model), (e) as obtained with the full layer model.

contact (cf. Fig. 4). So when there is a shock, it is not just one bead colliding with another bead, but a small upward column of beads colliding with a downward column of beads, the latter going down to the bottom. In this case the transfer of momentum is complex and depends on the angular position of the beads along these columns.

Simulating numerically this model gives the velocity profiles of Fig. 4 [2]. What we observe is precisely a flow only on the upper part for small tilt angle. The flow depth increases with the inclination angle, eventually reaching the bottom above a given one. The velocity profile looks very close to those observed experimentally (Fig. 5, (a) and (e), [11,12,19]): roughly a linear velocity profile, followed by a slow creeping tail. This slow deformation tail has been carefully studied in [20]. They have shown that it is an exponential with a characteristic length of 5 beads, independently of what is flowing above. This is very reminiscent of the exponential deformation observed in shear experiments. In other words it seems that we just observe a flowing layer with a linear velocity profile which shears an underneath static pile.

If we look at the velocity gradient of this linear velocity profile, we find that it corresponds simply to the velocity of a single bead above a static layer [2], roughly as if each layer of grain was rolling on a static underneath layer, with purely inelastic normal collisions [19]. This apparent inelasticity comes from the non-locality of the shocks: the momentum is transmitted down through the underneath column, so it looks as if it was dissipated, exactly as the momentum of a single bead is transmitted through the static bead, the plane, the table and the lab, down to the earth.

To further understand the selection of flow depth, we have to take into account the fact that one layer, to go above the underneath layer and fall into the next dip, has to lift up all the layers lying on top of it. In other words, the amplitude of the potential trapping is increasing linearly with depth. Now the shocks occurring above give to this layer only part of their momentum as some is still transmitted further down. The momentum transmitted thus increases with depth, but not as quickly as the trapping. So for a given angle, the condition that the shocks give enough momentum to pass the trapping selects a particular flowing depth.

This roughly linear velocity profile observed in surface flows seems to be in contradiction with experiments and numerical simulations of granular flows on rough planes, showing rather a Bagnold type of velocity profile [21–23]. A possible reduction of this discrepancy is to point out two differences: the chute experiments are done for angles largely above the ones at which surface flows are considered; the boundary condition (hard rough bottom) is very different from the soft plastically deforming pile. From both these differences an interpretation is then that chute flows are slightly more diluted than surface flows, so that the contact chains could then be finite in length, and we may recover a Bagnold type of velocity profile. A way to check this interpretation would be to look at the characteristic length in the stress expression (Eq. (5)) that can be derived from the velocity profile. This length should not be the grain diameter as in (5) but rather the typical chain length.

The presence of these contact chains giving rise to non-local shocks is precisely the idea underlying present models built to recover the characteristics of the chutes velocity profiles [24,25]. This is also the introduction of a non-local length scale (simply the local depth in the flow δ) in front of the Bagnold shear

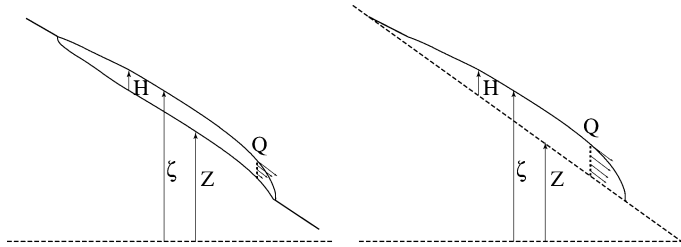


Figure 6. Sketch and notations for: (left) a surface flow over a thick static pile; (right) a flow down to a fixed bottom.

stress (replacing d^2 by $d\delta$), that allows Khakhar [8–10] to recover not only the linear velocity profile but also the good scalings.

4. Modeling

Looking at a single bead and layers of beads helps us to understand the hysteresis, the apparent forces, and the particular velocity profile. Now a macroscopic modeling of the whole surface flow can be made using the formalism first introduced by St-Venant [26], integrating the equations of motion vertically. In the case of a flowing layer as shown in Fig. 6, we obtain the general equations from the mass and momentum conservation:

$$\partial_t \zeta + \partial_x Q = 0, \quad (6)$$

$$\partial_t Q + \partial_x E = \frac{1}{\rho} F. \quad (7)$$

All the terms are vertical integrals: the free surface elevation ζ is the integral of 1, the flux Q of the velocity, the overall energy E of the velocity square and F of the resulting forces. These two equations are exact and quite general. All the particularities and approximations come from the various possible expressions of the different terms. In the case of a surface flow as in Fig. 6 left, the unknowns are: the free surface ζ , the flowing depth H and the mean velocity of the flowing layer U (simply related to the flux by $Q = UH$). We see that we have only two equations for three unknowns, so that at least one relation is missing.

4.1. Fixed bottom

A first solution is to consider flows down to a known fixed bottom Z (Fig. 6, right). Then the free surface is directly linked to the flowing height, $\zeta = Z + H$, and the two previous equations are enough to find the two remaining unknowns H and U . The first equation (6) gives the flowing depth H . The second one (7) gives the mean velocity U , using that $\partial_t Q = H \partial_t U + U \partial_t H$ and that $\partial_t H$ is given by the first equation.

Historically this modeling was first used to study flood waves in rivers. In this case the flux Q is assumed to be known as a function of the local flowing height (derived from the local cross sections of the river and/or flow calibrations). Then only the first mass conservation equation (6) is sufficient to solve the problem, with the characteristics method for instance [27].

Another classical use of these equations is for thin fluid layers. A first case is to assume a purely inviscid fluid ('the shallow water approximation'). Then the velocity profile is a constant one (plug flow), the fluid layer just sliding as a whole on the bottom (so $E = U^2 H$). The force is just derived from gravity and pressure (with at this place approximations of a thin slowly varying layer). A second case is on the contrary to assume a very viscous fluid ('the lubrication theory'). The velocity profile is then half of a parabola (with curvature given by viscosity), as shown in Fig. 5(b), and there is a viscous force added.

This fixed bottom approximation was also used in the case of granular flows. A first model by Savage and Hutter [4] is similar to the shallow water approximation (plug flow), except that a friction force between the flowing layer and the bottom is added. Pouliquen [5,28] has further refined this model by putting an

effective force derived from his measurements of granular flows on a rough plane. This is very similar to the flood wave studies, using measurements in constant stable flows to predict non-uniform flows.

4.2. Free bottom (thick pile)

Few models has been written for the case of a flow on an otherwise static pile. A first one was proposed by BCRE [6], and later modified by BRdG [7]. As in the previous models, it assumes a plug flow (constant velocity profile). However, there still remains three unknowns. So the velocity itself is assumed to be constant. Equation (6) then gives an equation for the free surface ζ and Eq. (7) for the flow depth H , as now $\partial_t Q = U \partial_t H$. In other words, if the flowing layer wants to gain (lose) momentum, it simply increases (decreases) its thickness. The model was not presented in this way, so that the left part of the second equation was not recognized as deriving from a physical force. However, it corresponds roughly to a constant friction force.

For our part, we proposed [3], as well as Khakhar [8–10], a model using experimental results as those described above. So we rather assume a linear velocity profile [29]. Then, as above, we need another relation, to determine one unknown. So we assume that the velocity gradient Γ is locally constant and equal to that of a single bead in the same local conditions (Fig. 3). We thus relate the mean velocity to the flowing depth, $U = \frac{1}{2}\Gamma H$, and $E = \frac{1}{3}\Gamma^2 H^3 = \frac{4}{3}U^2 H$. If the flowing layer wants to gain (lose) momentum, it now increases (decreases) both its mean velocity and depth, keeping its local velocity gradient unchanged. We also assume directly a hysteresis between static and dynamical friction forces with a typical transition depth (Fig. 7).

With these assumptions, the model summarizes into:

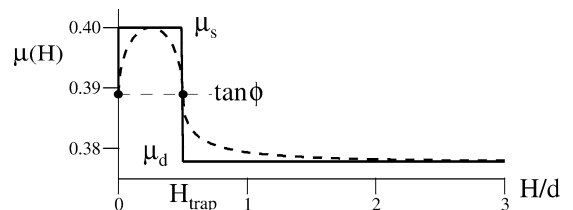
$$\partial_t \zeta + 2U \partial_x H = 0, \quad (8)$$

$$\partial_t H + 2U \partial_x H = \frac{g}{\Gamma(\psi)} (\tan \phi - \mu(H)), \quad (9)$$

with $U = 1/2\Gamma H$, $\Gamma(\psi)$ as shown in Fig. 3, and $\mu(H)$ as in Fig. 7, and ϕ the local surface slope. In this model we thus have essentially five parameters: H_{trap} , $\mu_s = \tan \phi_s$, μ_d , ϕ_∞ and γ (in (2)). For the moment we choose to have $\tan \phi_d$ (from Fig. 3) slightly smaller than μ_d (from Fig. 7), so that a flow stops essentially by reducing its flowing height, rather than by reducing its velocity gradient, but it may be chosen otherwise. The factor 2 in the advective terms comes from the linear velocity profile. This assumption of a linear velocity profile has direct influences on the expression of the flux and mean velocity height dependences. This in turn have strong effects on the results, as exemplified in [29].

This model can be checked in the case of stationary flows. This is what is done by Khakhar [8–10], but also Bonamy [11,12], for instance, with encouraging results. However, we also want to check it for more demanding cases, namely transients and unstable situations. A first work is about avalanches on a rough plane [13,14], a second one on fronts in a half flat hourglass [15].

Figure 7. Variation of the friction coefficient with flowing depth. Below a trapping height H_{trap} , of the order of one grain diameter, the friction coefficient exchanges from dynamical to static.



5. Experiments and comparisons

5.1. Avalanches on a rough plane

A rough plane creates a particular boundary effect: the dynamical (and static) friction seem to increase when going close to this rough plane. It may come from the fact that the plane roughness is frozen, contrary to that of a sand pile that can still be sheared. It results in a fact that, when some granular material flows on the plane, it can remain a fixed layer of grains with a well defined height when the flow stops, even for a plane inclination larger than the dynamical angle of the granular material used [28].

Now this layer of grains is particularly stable at this angle (the dynamical angle for this particular height). This layer remains stable even if the plane is further tilted, by an angle $\delta\phi$, up to another angle where it start to flow spontaneously (the static angle for this layer height). Between the two angles the layer is metastable, and a local perturbation can trigger an avalanche [13]. Depending on this tilt angle $\delta\phi$, we observe three regimes. For $\delta\phi = 0$, a mass of grains which is set into motion just propagates down as a droplet, leaving the plane unchanged except for small lateral ridges. For $\delta\phi > 0$ but small, we observe an avalanche gaining material while going down, and increasing its lateral extension linearly, leaving a triangular track. For a larger $\delta\phi$, there is an abrupt transition to another regime of propagation, the grain above the flowing part also starting to flow down (upward front propagation), so that eventually all the plane flows (see Fig. 8).

To simulate these avalanches, we use the model as presented above extended to 3D. To take into account the influence of the rough plane, we add for input the variation of the dynamical friction coefficient with the distance to the plane. The results are presented in Fig. 8. The results are qualitatively good on the shape of the flows. They are even quantitatively good on the various front velocities if the parameters are finely tuned.

5.2. Half flat hourglass

When sand is poured at the top of a pile with a small enough flux, it accumulates and eventually an avalanche starts going down. At one place, we observe the transition from a static surface to a flowing one,

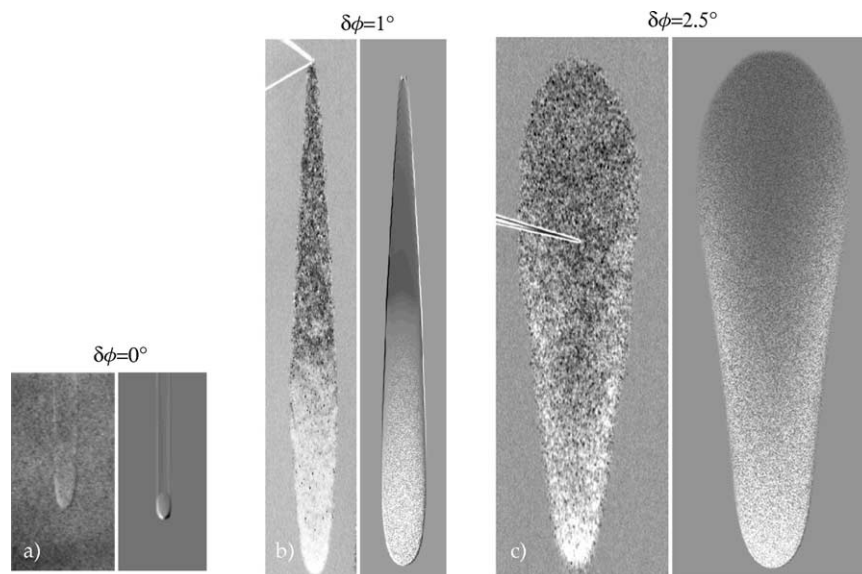


Figure 8. Image differences of the granular layer (left) and results of the numerical simulation of the model (right). (a) For no further tilt of the plane after preparation, $\delta\phi = 0$, we observe a droplet propagating down, leaving banks. (b) For a small $\delta\phi$, we observe a triangular avalanche; (c) and for larger $\delta\phi$, we observe an avalanche front also propagating upward. The pin in the experimental pictures points to the triggering place.

and the front is going down so we call this front the ‘start-down’ front (Fig. 9(a)). This is the front usually considered for avalanches. But when this front reaches the end of the pile, it spreads and stops. There is then a stopping front moving upward (Fig. 9(b)). When this ‘stop-up’ front reaches the top of the pile, the sand accumulates again and so we have successive avalanches starting down and stopping up.

If we make the symmetric of this classical experiment, i.e. a sand pile emptying at its lower end, we also observe two other fronts. The complete experiment, with an upper flat silo emptying and a lower one filling up, could be described as a ‘Half Flat Hourglass’ (Fig. 10). In the upper part, the sand goes out at the foot of the sandpile, and it creates an increasing step. When this step is steep enough, the upper static grains starts to roll down, and we observe a ‘start-up’ front (Fig. 9(c)). When it has reached the top end of the pile, it also flattens and stops. We then observe a ‘stop-down’ front (Fig. 9(d)). These four fronts are the four possible fronts either starting or stopping, either moving up or down. We find that they propagate at constant velocities.

These four fronts have different characteristics. The ‘start-down’ and ‘start-up’ fronts are sharp. We can also observe that they sharpen with time, but tends towards a fixed shape. On the other hand, the ‘stop-down’ and ‘stop-up’ fronts are flat, and flattening with time. These observations are already very restrictive for possible models.

We performed numerical simulation of our model proposed above. We recover, qualitatively for the moment, the good characteristics (see Fig. 11). The first is the existence of the four fronts. This is particularly true for the ‘stop-down’ front, which propagates down only because of H_{trap} . Next the linear velocity profile give the sharp shape of the of the two starting fronts, and the flattening of the two stopping fronts [15]. Further more, the ‘start-down’ front presents a well defined angle. In our model this angle is precisely the jumping angle ϕ_{∞} . Finally, the angle of the ‘start-up’ front is just the starting angle ϕ_s .

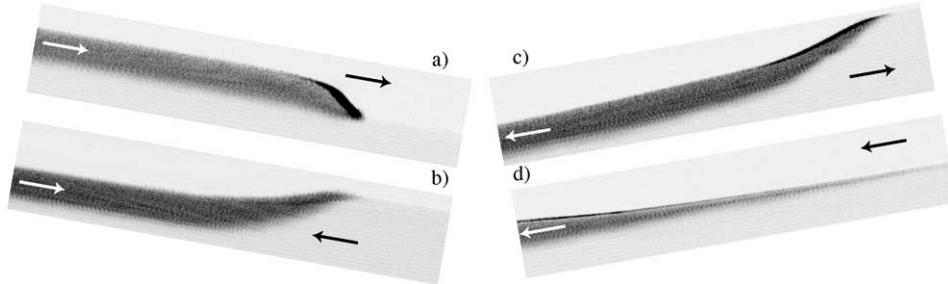


Figure 9. The four types of fronts as observed with image differences showing the flowing layer in dark grey. The white/black arrows indicate the grain/front motion, respectively.

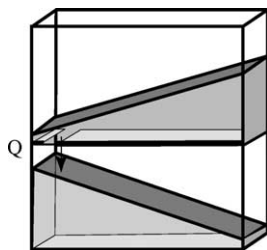


Figure 10. Sketch of the half flat hourglass experiment: the upper part is emptying into the lower part, with a fixed flux Q .

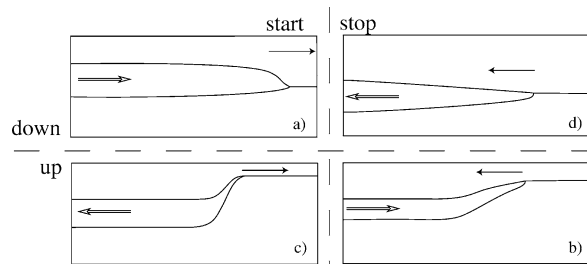


Figure 11. The four types of fronts as obtained with numerical integration of our model. (a)–(d) as in Fig. 9.

6. Conclusion

We have seen that looking at the motion of a single bead and layer of beads gives much information on granular surface flows. The first point is the presence of trapping of grains in the dip between the grains underneath. The second is that the complex grain motion results on the average to the hysteretic friction laws. The third is the non-locality of the shocks in dense slow flows, as all the grains are in permanent contact. The fact that for a larger angle, a more rapid flow, or a different bottom, the contact line may become finite and small could explain the difference between the velocity profiles observed for surface flows and chute flows. This points deserve further investigation.

The St-Venant approach seems to be satisfactory in the case of stationary granular surface flows if the hypothesis of a linear velocity profile with a velocity gradient given by the velocity of one grain is used. Its results are also compatible with more demanding cases such as the four avalanche fronts and the avalanches on a rough plane. The next work is to make a quantitative comparison of different experiments with the same material (parameters.) Finally, a more distant goal would be to see how far these type of models can be extended, in particular in the case of geological flows. Is the inertial effect already present with the advective term derived from a linear velocity profile enough to describe these huge flows, or are further modifications needed?

References

- [1] L. Quartier, B. Andreotti, A. Daerr, S. Douady, *Phys. Rev. E* 62 (2000) 8299.
- [2] B. Andreotti, S. Douady, *Phys. Rev. E* 63 (2001).
- [3] S. Douady, B. Andreotti, A. Daerr, *Eur. Phys. J. B* 11 (1999) 131.
- [4] S.B. Savage, K. Hutter, *J. Fluid Mech.* 199 (1989) 177.
- [5] O. Pouliquen, *Phys. Fluids* 11 (1999) 1956.
- [6] J.P. Bouchaud, M. Cates, J.R. Prakash, S.F. Edwards, *J. Phys. France I* 4 (1994) 1383.
- [7] T. Boutreux, E. Raphael, P.G. de Gennes, *Phys. Rev. E* 58 (1998) 4692.
- [8] D.V. Khakhar, J.J. Mac Carthy, J.J. Shinbrot, J.M. Ottino, Transverse flow and mixing of granular materials in a rotating cylinder, *Phys. Fluids* 9 (1997) 31.
- [9] D.V. Khakhar, A.V. Orpe, P. Andersén, J.M. Ottino, *J. Fluid Mech.* 441 (2001) 255.
- [10] D.V. Khakhar, A.V. Orpe, J.M. Ottino, preprint, <http://www.ictp.trieste.it/~web1322/khakhar.ps>.
- [11] D. Bonamy, B. Faucherand, M. Planelles, F. Daviaud, L. Laurent, in: Y. Kishino (Ed.), *Powder and Grains 2001*, Balkema, Amsterdam, 2001, p. 463.
- [12] D. Bonamy, F. Daviaud, L. Laurent, *Phys. Fluids*, to appear.
- [13] A. Daerr, S. Douady, *Nature* 399 (1999) 6733.
- [14] A. Daerr, *Phys. Fluids* 13 (2001) 2115.
- [15] S. Douady, B. Andreotti, A. Daerr, P. Cladé, in: Y. Kishino (Ed.), *Powders and Grain 2001*, Balkema, Amsterdam, 2001, p. 443.
- [16] C.D. Jan, H.W. Shen, C.H. Ling, C.L. Chen, in: *Proc. 9th Conf. on Eng. Mech.*, College Station, Texas, 1992, p. 768.
- [17] G.H. Ristow, F.X. Rigidel, D. Bideau, *J. Phys. I France* 4 (1994) 0.
- [18] R.A. Bagnolds, *Proc. R. Soc. London Ser. A* 295 (1966) 219.
- [19] J. Rajchenbach, in: Hermann, Hovi, Luding (Eds.), *Physics of Dry Granular Media*, Kluwer, Netherlands, 1998, p. 421.
- [20] T.S. Komatsu, S. Inagaki, N. Nakagawa, N. Nasuno, *Phys. Rev. Lett.* 86 (2001) 1757.
- [21] C. Ancey, P. Evesque, P. Coussot, *J. Phys. I France* 6 (1996) 725.
- [22] E. Azanza, F. Chevoir, P. Moucheron, *J. Fluid Mech.* 400 (1999) 199.
- [23] M. Prochnow, F. Chevoir, M. Albertelli, in: *13th Int. Conf. on Rheology*, Cambridge, 2000.
- [24] P. Mills, D. Loggia, M. Tixier, *Europhys. Lett.* 45 (1999) 733.
- [25] J. Jenkins, F. Chevoir, preprint, 2001.
- [26] A.J.C. de Barré Saint-Venant, *C. R. Acad. Sci. Paris* 31 (1850) 283.
- [27] G.B. Whitham, *Linear and Nonlinear Waves*, Wiley, 1974.
- [28] O. Pouliquen, *Phys. Fluids* 11 (1999) 542.
- [29] A. Aradian, E. Raphael, P.-G. de Gennes, *Phys. Rev. E* 60 (1999) 2009.